Geophys. J. Int. (2002) **148,** F1–F5

FAST TRACK PAPER

Potency-magnitude scaling relations for southern California earthquakes with $1.0 < M_L < 7.0$

Yehuda Ben-Zion[1,*] and Lupei Zhu[2]

[1] *Department of Earth Sciences, University of Southern California, Los Angeles,* CA 90089. *E-mail: benzion@terra.usc.edu*
[2] *Department of Earth and Atmospheric Sciences, Saint Louis University, St. Louis,* MO 63103

Accepted 2001 November 8. Received 2001 October 10; in original form 2001 July 23

SUMMARY

Linear and quadratic scaling relations between potency P_0 and local magnitude M_L for southern California earthquakes are derived using observed data of small events ($1.0 < M_L < 3.5$) recorded in the Cajon Pass borehole and moderate events ($3.5 < M_L < 6.0$) recorded by the broad-band TERRAscope/TriNet network. The derived relations are extended to $M_L = 7.0$ and compared with observed potency–magnitude values of four earthquakes in the extended range. The results indicate that a linear scaling relation can describe accurately data extending only over 2–3 orders of magnitudes. The best-fitting slope of a linear $\log P_0$ vs M_L scaling for the small Cajon Pass events is about 1.0, while the slope for the $3.5 < M_L < 6.0$ events is about 1.34. A quadratic relation can fit the data well over the entire $1.0 < M_L < 7.0$ magnitude range. The results may be explained in terms of a continuous transition from a limiting scaling $P_0 \sim$ (rupture area) for highly disordered small events, to a limiting scaling $P_0 \sim$ (rupture area times slip) for crack-like large events. Such a transition is expected to characterize evolving seismicity on heterogeneous faults, where small events propagate in (and are arrested by) a rough fluctuating stress field, while large events propagate across a relatively smooth correlated field.

Key words: earthquakes, fault models, seismicity, seismic stress.

1 INTRODUCTION

Earthquake sizes are most commonly quantified with various types of magnitudes associated with spectral amplitudes of radiated seismic energy at a given frequency band (and accepted site and instrument conditions). For example, the local magnitude M_L is based on waves near 1 Hz recorded by a Wood–Anderson seismograph at a site with a competent rock and epicentral distance of 100 km (e.g. Richter 1935). The magnitudes are relatively easy to measure and they give information that is directly useful for various engineering applications (e.g. the response of structures with resonance frequencies near those used to define the magnitude). However, for large earthquakes they reflect radiation from subportions of the rupture rather than giving a physical characterization of the entire earthquake source. The latter is provided by the zero frequency asymptote of the displacement source spectrum, which is proportional (e.g. Aki & Richards 1980) to the integral

$$P_0 = \int_A u \, dA, \tag{1}$$

where u is slip, A is rupture area and P_0 is called geometric moment by King (1978) and potency by Ben-Menahem & Singh (1981). Here we use the term potency for P_0.

Because of historical developments, seismologists typically use the related quantity seismic moment

$$M_0 = \mu P_0, \tag{2}$$

where μ is shear rigidity at the source, instead of the potency. As summarized by Ben-Zion (2001), however, the potency is a better scaling parameter for the overall size of a slip event, as it is the directly observable quantity whereas the compound parameter, moment, involves assumptions on material properties at the source. The significance of this seemingly small difference may be better appreciated upon realizing that material properties have rapid spatio-temporal variations in the space–time domains associated with earthquake sources and hence are ambiguously defined precisely where they are needed for eq. (2).

In this work we derive potency–magnitude scaling relations in the form

$$\log P_0 = \gamma M^2 + cM + d, \tag{3}$$

*Contact: 213 740 6734; Fax +1 213 740 8801.

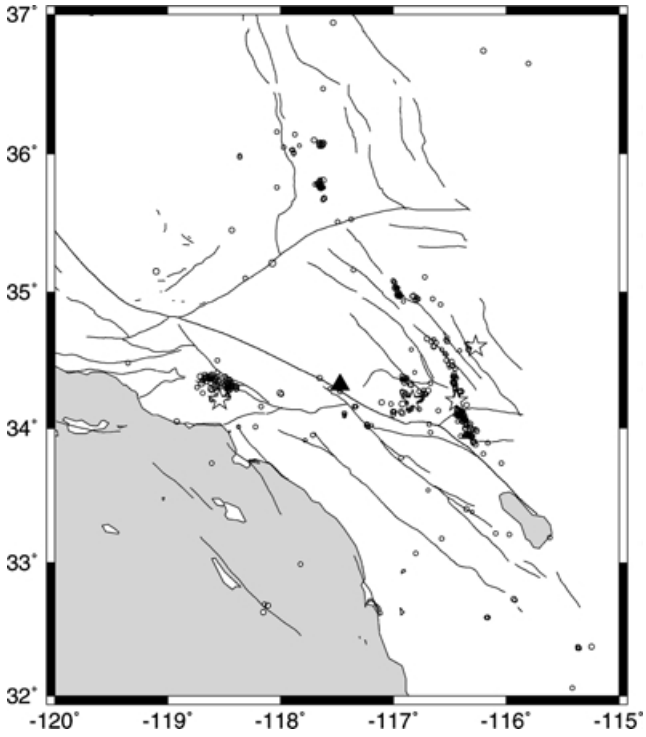

Figure 1. Locations of the Cajon Pass borehole (triangle), 418 moderate earthquakes (open circles with sizes proportional to M_L), and the 1992 Landers and Big Bear earthquakes, 1994 Northridge earthquake and 1999 Hector Mine earthquake (stars).

for earthquakes in southern California (Fig. 1) using two data sets. The first, based on Zhu & Helmberger (1996) and augmented by analysis of additional events, consists of 418 earthquakes in the range $3.5 < M_L < 6.0$ recorded by the TERRAscope/TriNet network. The second, taken from Abercrombie (1996), consists of 18 earthquakes of $1.0 < M_L < 3.5$ recorded in the deep Cajon Pass borehole. A third set with four earthquakes of $6.0 < M_L < 7.0$, not employed in the derivation of the coefficients in eq. (3), is used to assess the performance of the obtained relations based on the first two data sets.

The results indicate that the values of c and d for the first and second data sets are significantly different. The best-fitting linear slope for the $M_L < 3.5$ events is $c \sim 1$, while for the $M_L > 3.5$ events it is $c \sim 1.34$. The lack of a single linear relation for earthquakes in the combined magnitude range is compatible with the observational and theoretical moment–magnitude analysis of Hanks & Boore (1984), the observational moment–magnitude work of Bakun (1984) and the synthetic seismicity and stress simulations of Ben-Zion & Rice (1993), Ben-Zion (1996) and Miller *et al.* (1999). The quadratic term in eq. (3) is not significant over the five orders of magnitudes of the first and second data sets. However, extrapolations of the best-fitting results from those data to larger events and examination of observed potency–magnitude values of the four additional $M_L > 6.0$ events indicates, in agreement with Hanks & Boore (1984), that a quadratic term is required for fitting data spanning a broad magnitude range with a single scaling relation. Hanks & Boore (1984) explained the quadratic scaling in terms of observational artefacts associated with different combinations of bandwidths characterizing the Wood–Anderson seismometer and a source model with constant stress drop and 'ω-square' spectrum. The observed scaling variation with increasing event size may also be explained by assuming that the occurrence of increasingly larger events is associated with increasingly smoother stress fields. Actual data may have signatures of all these effects.

2 ANALYSIS

The M_L values of all used earthquakes are determined by the Southern California Short-period Network (SCSN). The moments and potencies of the 418 events (Fig. 1) with $3.5 < M_L < 6.0$ were obtained by inverting their broad-band regional waveforms using the CAP source estimation technique (Zhu & Helmberger 1996). This method uses a regional velocity model to calculate the Green's functions and compares synthetics with observed waveforms to estimate source depths and potency/moment tensors. One advantage of this technique over other source estimation methods is that in the inversion it employs the body and surface wave portions of the seismograms separately. This allows the inversion to put more weight on the stable body wave portion to reduce the influence of shallow crustal heterogeneities. The amplitude ratio between the body and surface waves provides a constraint on the source depth. The originally-derived moments of Zhu & Helmberger (1996) were converted to potencies by dividing each moment value with the rigidity assumed in the moment estimation procedure. Using the CAP technique, it is possible to determine the potency/moment of earthquakes down to M_L magnitude of about 3.5.

The scalar moments of the 18 small events in the second data set were obtained by Abercrombie (1996) from the low frequency asymptotes of their displacement spectra, converted to seismic moments using the whole-space displacement formula and assuming a mean radiation pattern (Aki & Richards 1980). The moments were again divided by the rigidity values assumed in the moment estimation procedure (Abercrombie, personal communication 2001) to obtain potencies.

Removing the assumed rigidities in the different data sets allows us to treat the combined data more uniformly and to derive potency–magnitude scaling relations of the type given by eq. (3). This is done by fitting a linear or a quadratic relation to a given set of potency–magnitude values using the least-squares method. In the linear case, the least-squares method minimizes for the employed data points the quantity

$$\Phi = \sum_{i=1}^{n} \left(\log P_0^i - c M_L^i - d \right)^2. \tag{4}$$

An analogous quantity is minimized for the quadratic case. The goodness of the fit may be estimated by

$$\chi_\nu^2 = \frac{\Phi_{min}}{(n-2)\sigma^2}, \tag{5}$$

where σ^2 is the standard deviation of the P_0 values. In our data not only P_0 but also M_L have measurement uncertainties that are not known *a priori*. We thus treat the above σ^2 as a combined standard deviation of both quantities. It can be estimated from the data at the expense of loosing the ability of evaluating the goodness of fit (Bevington & Robinson 1992). This amounts to assuming $\chi_\nu^2 = 1$ from which

$$\sigma^2 = \frac{\Phi_{min}}{(n-2)}. \tag{6}$$

We first fit the two different data sets separately with linear relations. The results are summarized and shown in Table 1 and Fig. 2.

Table 1. Parameters from linear least-squares fits. The uncertainties are estimated using $\sigma = 0.24$ obtained from eq. (6).

	$M_L < 3.5$	$M_L > 3.5$
n	18	418
c	1.00 ± 0.11	1.34 ± 0.02
d	-4.72 ± 0.22	-5.22 ± 0.10

Table 2. Parameters from linear and quadratic least-squares fits for combined data with $1.0 < M_L < 6.0$.

	Linear	Quadratic
c	1.35 ± 0.03	0.988 ± 0.213
d	-5.33 ± 0.06	-4.87 ± 0.25
γ		0.0612 ± 0.0385

The two data sets have considerably different slopes, in agreement with the observational results of Bakun (1984) for central California earthquakes. However, the difference may result, at least in part, from the fact that the second data set of low magnitude events contains only 18 measurements and the two data points near $M_L \sim 3$ have a strong influence on the result. A single linear fit of the combined data set is discussed next. We note that both slopes ($c \sim 1$ and $c \sim 1.34$) are significantly different from the usually assumed value of 1.5 (Kanamori 1977; Hanks & Kanamori 1979). A slope of 1.5 is expected theoretically for a classical crack model with a constant stress drop (e.g. Kanamori & Anderson 1975). However, the expected value for a disordered failure process in a fluctuating stress field is lower (Fisher *et al.* 1997).

Hanks & Boore (1984) presented observational and theoretical evidence for a continuous positive curvature of the $\log M_0$ vs M_L relation for California earthquakes in the magnitude range $0 < M_L < 7.0$. The theoretical results were based on numerical simulations of far-field shear-wave acceleration with finite-duration band-limited white Gaussian noise (Boore 1983). To examine whether non-linearity is present in our data, we fit single linear and quadratic relations to the combined data set. To have similar sample sizes in the different magnitude ranges, we combine the 18 points of the second data set with 20 randomly selected points from the first set. (If we simply fit all the points of the combined data, the results will be dominated by properties of the first set as it has a much larger number (418) of events than that (18) of the second.)

We then perform linear and quadratic least-squares fits to the 38 points over the magnitude range $1.0 < M_L < 6.0$. This is repeated 500 times with different randomly selected points. The mean and standard deviations of the best-fitting parameters in the 500 realizations are given in Table 2. The best-fitting lines and the quadratic theoretical relation of Boore (1983) are plotted in Fig. 3. The slopes of the linear fit (dotted line, $c \sim 1.35$) and quadratic relation (solid line, $c + 2\gamma M_L \sim 1.42$ for a mid-range magnitude $M_L = 3.5$) are again different from the usually assumed 1.5 value.

Given the relatively small number of events, it is not very meaningful to discuss which of the three relations plotted in Fig. 3 is statistically the best. Instead, the relative performance of the three lines can be assessed by examining how well extrapolations of the relations to a higher (or lower) magnitude range can fit independent data points in the extended range. The circles in the upper right corner of Fig. 3 give, from bottom-left to upper-right, P_0 and M_L values of the 1992 Big Bear, 1994 Northridge, 1999 Hector Mine and 1992 Landers California earthquakes (Fig. 1). The potency values are derived using the CAP technique of Zhu & Helmberger (1996) and TERRAscope/TriNet waveform data. The local magnitudes are obtained from synthetic Wood–Anderson amplitudes based on observed broad-band seismograms (K. Hutton, personal communication 2001). The additional data points fall

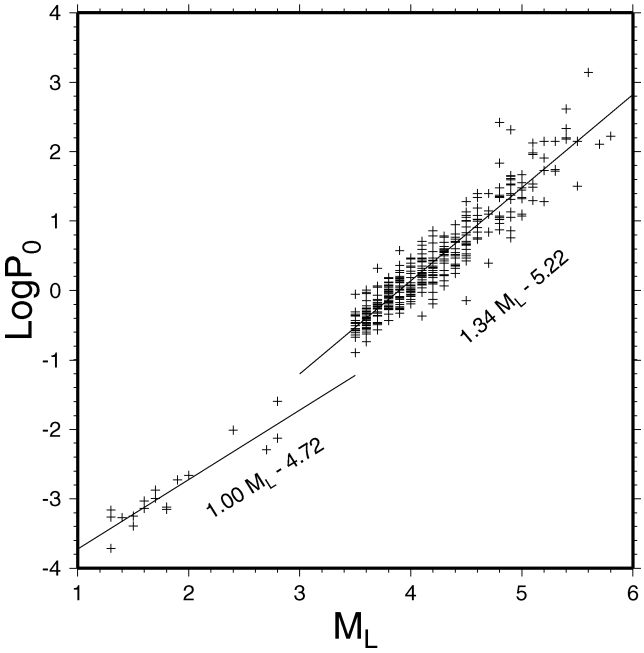

Figure 2. Linear least-squares fits done separately for the $18 M_L < 3.5$ and $418 M_L > 3.5$ events. The best-fitting parameters are summarized in Table 1. Potency values are in cm km^{-2}.

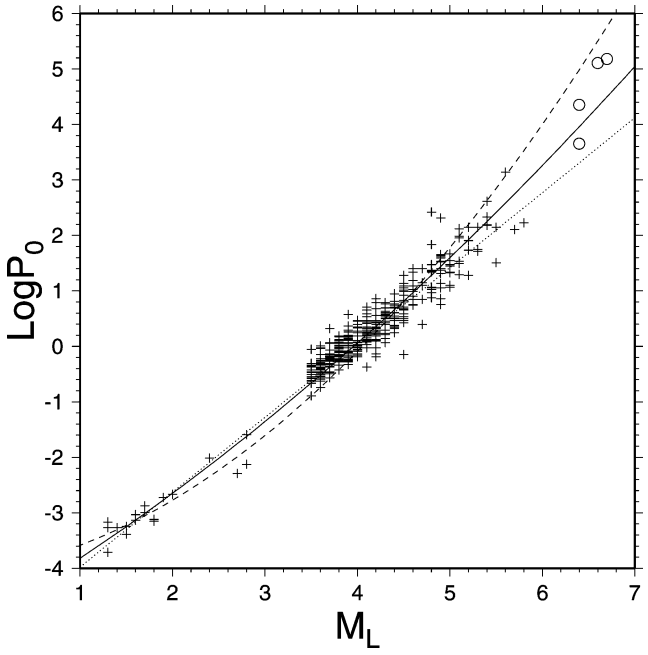

Figure 3. Least-squares fits with linear (dotted line) and quadratic (solid line) relations based on 500 realizations of a combined data set including the $18 M_L < 3.5$ and 20 randomly selected $M_L > 3.5$ events. The best-fitting parameters are summarized in Table 2. The dashed line is based on the model calculations of Boore (1983). The circles give values of 4 events not used to produce the fits. See text for more.

between or near the quadratic theoretical relation of Boore (1983) and the quadratic least-squares fit based on the $1.0 < M_L < 6.0$ events. The linear least-squares fit based on the $1.0 < M_L < 6.0$ events clearly underestimates the potency values of most larger earthquakes. The same holds for the line based on the $M_L > 3.5$ events in Fig. 2, as its slope is almost the same (and slightly below) that of the linear fit of Fig. 3. The results indicate, in agreement with Hanks & Boore (1984), that the quadratic term in eq. (3) is required for describing the scaling between potency and magnitude values over a broad range of sizes with a single relation. A linear potency–magnitude scaling relation can approximate only a limited range of data.

3 DISCUSSION

The scaling relation between observed potency and magnitude values of earthquakes has important implications for a variety of theoretical and applied studies, ranging from proper understanding of the underlying processes to calculations of co-seismic strain and seismic hazard associated with the ongoing seismicity. Using the borehole seismic data of Abercrombie (1996) for $1.0 < M_L < 3.5$ events and broad-band TERRAscope/TriNet data for $3.5 < M_L < 6.0$ events, we derive linear and quadratic potency–magnitude scaling relations for southern California earthquakes. The derived relations are extended to higher potency–magnitude values and compared, along with the theoretical quadratic curve of Boore (1983), with four independent data points with $6.0 < M_L < 7.0$.

The coefficients obtained by separate linear least-squares fits for the $M_L < 3.5$ and $M_L > 3.5$ events (Table 1 and Fig. 2) show a significant change of slope, from $c \sim 1$ in the first magnitude range to $c \sim 1.34$ in the second. These results should be substantiated with additional data points near $M_L = 3.5$. Fitting the data over the combined magnitude range with a single scaling relation requires a quadratic term. The derived scaling relations are compatible with the observations of Bakun (1984) for central California earthquakes and Hanks & Boore (1984) for a compilation of Californian events. This supports the assertion of Hanks & Boore (1984) that there is no fundamental regional dependence in the potency/moment–magnitude scaling relation of earthquakes.

Hanks & Boore (1984) explained the observed non-linear scaling as resulting from different interactions between M_L measurements, dominated by the 1.25 Hz natural frequency of a Wood–Anderson instrument, and a constant stress drop 'ω-square' model. In this explanation, M_L values of small earthquakes reflect the constant low-frequency portion of the source radiation, while M_L values of large events reflect the high-frequency fall-off of the source spectrum. Below, we suggest a possible alternative explanation, motivated by numerical modelling of seismicity on strongly heterogeneous faults with highly fluctuating stress fields, not affected by observational artefacts.

Ben-Zion & Rice (1993) simulated earthquake patterns along a 2-D discrete fault zone with strong fixed heterogeneities in a 3-D elastic half-space. The slope of the log P_0 vs log A of the simulated small events was $c \sim 1$, while the slope for the moderate events was $c \sim 1.5$. (The transition between the two groups was near $M = 4.9$, but this is not significant since the magnitudes in the discrete model of Ben-Zion and Rice are grid-size-dependent and smaller grid would have shifted the results to lower magnitudes.) Miller *et al.* (1999) simulated seismicity patterns along a similar discrete fault zone model having evolving strength heterogeneities due to evolving pore pressure distribution. The results in that model had a gradual transition of scaling, from a relatively diffused region of small events bounded by $M_0 \sim A$ to a relatively narrow region with $M_0 \sim A^{\frac{3}{2}}$ for intermediate events. The simulation results of both models are similar to the observations of Figs 2 and 3, and those of Bakun (1984) and Hanks & Boore (1984), assuming $M \sim \log A$ as indicated by observations (Kasahara 1981; Wells & Coppersmith 1994).

The transitions of scaling in the modelling results, and perhaps also in nature, are associated with complementary aspects of stress field evolution at short and long length scales (Ben-Zion 1996). The simulated small events create, and typically grow in, a stress field with strong stress fluctuations over short distances. On the other hand, the large earthquakes occur only when the stress, generated by the collective occurrence of the small events and the gradual tectonic loading, is relatively smooth and correlated over large distances (see also Ben-Zion & Lyakhovsky 2001; Sammis & Sornette 2001). In such a stress field, small events are strongly affected by the short scale stress fluctuations and have slip that does not grow substantially with the rupture dimension. The limiting scaling for highly disordered fractal-like ruptures is $P_0 \sim A$ (Fisher *et al.* 1997). In contrast, large earthquakes grow in a relatively homogeneous stress field and they average out the remaining short scale fluctuations over their (large) rupture areas. The limiting scaling for such cases is the classical smooth crack relation $P_0 \sim A^{\frac{3}{2}}$ (e.g. Kanamori & Anderson 1975).

In the model of Ben-Zion & Rice (1993) with fixed strong heterogeneities, the transition between the above two limiting scaling regimes is relatively sharp. In the model of Miller *et al.* (1999) with evolving heterogeneities, the transition is more gradual. The scaling relation of seismicity on heterogeneous faults with a broad range of size scales and gradual evolution of strength properties is expected to have a continuous positive curvature of the type shown in Fig. 3 and in Hanks & Boore (1984). Further clarification of the true potency–magnitude relation of earthquakes will require additional observational and theoretical work.

ACKNOWLEDGMENT

We thank Rachel Abercrombie for providing the moment, magnitude and assumed rigidity values of the $M < 3.5$ events, Kate Hutton for providing the local magnitude values of the $M > 6$ events and Hiroo Kanamori for informative discussions. The manuscript benefitted from useful comments by Bill Foxall and an anonymous reviewer. The work was supported by the Southern California Earthquake Center (based on NSF cooperative agreement EAR-8920136 and USGS cooperative agreement 14-08-0001-A0899). LZ was also supported by a USGS NEHRP grand (00HQGR0007).

REFERENCES

Abercrombie, R.E., 1996. The magnitude-frequency distribution of earthquakes recorded with deep seismometers at Cajon Pass, southern California, *Tectonophysics,* **261,** 1–7.

Aki, K. & Richards, P.G., 1980. *Quantitative Seismology, Theory and Methods,* Freeman and Company, San Francisco.

Bakun, W.H., 1984. Seismic moments, local magnitudes, and coda-duration magnitudes for earthquakes in central California, *Bull. seism. Soc. Am.,* **74,** 439–458.

Ben-Menahem, A. & Singh, S.J., 1981. *Seismic Waves and Sources,* Springer-Verlag, New York.

Ben-Zion, Y., 1996. Stress, slip and earthquakes in models of complex single-fault systems incorporating brittle and creep deformations, *J. geophys. Res.,* **101,** 5677–5706.

Ben-Zion, Y., 2001. A note on quantification of the earthquake source, *Seism. Res. Lett.,* **72,** 151–152.

Ben-Zion, Y. & Lyakhovsky, V., 2001. Accelerated seismic release and related aspects of seismicity patterns on earthquake faults, *Pure appl. Geophys.,* **in press**.

Ben-Zion, Y. & Rice, J.R., 1993. Earthquake failure sequences along a cellular fault zone in a three-dimensional elastic solid containing asperity and nonasperity regions, *J. geophys. Res.,* **98,** 14 109–14 131.

Bevington, P.R. & Robinson, D.K., 1992. *Data Reduction and Error Analysis for the Physical Sciences,* McGraw-Hill Inc, New York.

Boore, D.M., 1983. Stochastic simulation of high-frequency ground motions based on seismological models of the radiated spectra, *Bull. seism. Soc. Am.,* **73,** 1865–1894.

Fisher, D.S., Dahmen, K., Ramanathan, S. & Ben-Zion, Y., 1997. Statistics of earthquakes in simple models of heterogeneous faults, *Phys. Rev. Lett.,* **78,** 4885–4888.

Hanks, T.C. & Boore, D.M., 1984. Moment-magnitude relations in theory and practice, *J. geophys. Res.,* **89,** 6229–6235.

Hanks, T.C. & Kanamori, H., 1979. A moment magnitude scale, *J. geophys. Res.,* **84,** 2348–2350.

Kanamori, H., 1977. The energy release in great earthquakes, *J. geophys. Res.,* **82,** 2981–2987.

Kanamori, H. & Anderson, D.L., 1975. Theoretical basis of some empirical relations in seismology, *Bull. seism. Soc. Am.,* **65,** 1073–1095.

Kasahara, K., 1981. *Earthquake Mechanics,* Cambridge University Press, Cambridge.

King, G.C.P., 1978. Geological faults, fractures, creep and strain, *Phil. Trans. R. Soc. Lond.,* A., **288,** 197–212.

Miller, S.A., Ben-Zion, Y. & Burg, J.-P., 1999. A three-dimensional fluid-controlled earthquake model: behaviour and implications, *J. geophys. Res.,* **104,** 10 621–10 638.

Richter, C.F., 1935. An instrumental earthquake scale, *Bull. seism. Soc. Am.,* **25,** 1–32.

Sammis, C.G. & Sornette, D., 2001. Positive feedback, memory and the predictability of earthquakes, *Proc. Nat. Acad. Sci. USA,* **in press**.

Wells, D.L. & Coppersmith, K.J., 1994. New empirical relationships among magnitude, rupture length, rupture width, rupture area, and surface displacement, *Bull. seism. Soc. Am.,* **84,** 974–1002.

Zhu, L. & Helmberger, D.V., 1996. Advancement in source estimation techniques using broad-band regional seismograms, *Bull. seism. Soc. Am.,* **86,** 1634–1641.